Potassium-mediated bacterial chemotactic response

Chi Zhang, Rongjing Zhang, Junhua Yuan

Hefei National Research Center for Physical Sciences at the Microscale and Department of Physics, University of Science and Technology of China, Hefei, Anhui 230026, China.

Corresponding authors:

Junhua Yuan, Rongjing Zhang or Chi Zhang, Hefei National Laboratory for Physical Sciences at the Microscale and Department of Physics, University of Science and Technology of China, Hefei, Anhui, 230026, China, tel +86-551-63600851, email: jhyuan@ustc.edu.cn; rjzhang@ustc.edu.cn; zhchi@ustc.edu.cn.

Abstract

Bacteria in biofilms secrete potassium ions to attract free swimming cells. However, the basis of chemotaxis to potassium remains poorly understood. Here, using a microfluidic device, we found that *Escherichia coli* can rapidly accumulate in regions of high potassium concentration on the order of millimoles. Using a bead assay, we measured the dynamic response of individual flagellar motors to stepwise changes in potassium concentration, finding that the response resulted from the chemotaxis signaling pathway instead of the motor response to changes in the proton motive force (PMF). To characterize the chemotactic response to potassium, we exposed the bacteria to a range of potassium concentrations and measured the dose-response curve and adaptation kinetics via a FRET assay, finding that the chemotaxis pathway exhibited a sensitive response and fast adaptation to potassium. We further found that the two major chemoreceptors Tar and Tsr respond differently to potassium. Tar receptors exhibit a biphasic response, whereas Tsr receptors respond to potassium as an attractant. These different responses were consistent with the responses of the two receptors to intracellular pH changes. Therefore, bacteria may sense the change in potassium concentration by sensing the change in intracellular pH. The sensitive response and fast

adaptation allow bacteria to sense and localize small changes in potassium concentration. As the ratio of the two major chemoreceptors changes with bacterial growth stages, the differential responses of Tar and Tsr receptors to potassium suggest that cells at different growth stages respond differently to potassium and may have different requirements for potassium.

Introduction

Potassium is an important ion in the normal physiological process of organisms [1]. Potassium ions are a major component in establishing the resting membrane potential and thus ensure proper function of the muscles and nerves. Potassium deficiency can affect many biological functions, such as human heartbeat [2] and photosynthesis and respiration of plants [3]. In prokaryotes, such as bacteria, potassium ions play a critical role in maintaining the osmotic pressure, pH value and membrane potential of cells [4,5]. In addition, both the expression of genes and the activities of enzymes are also regulated by potassium ions [4-7].

Because of its central role in maintaining the normal physiological state of cells, organisms have evolved a series of regulatory systems to control the intracellular concentration of potassium ions, such as Na^+/K^+ ATP pumps in higher organisms and potassium transport systems in prokaryotes. Most of the studies on potassium have focused on its effects on cell physiology or the dynamics of potassium transport systems. In contrast, studies on the behavioral response to environmental potassium concentration changes and the signaling pathways involved are very limited for bacteria.

Bacteria sense and respond to chemicals via the chemotaxis signaling pathway. In *E. coli*, chemo stimuli are detected by transmembrane receptors [8-10]. The sensed signal is then transmitted to the associated cytoplasmic histidine kinase CheA, affecting its autophosphorylation [11,12]. CheA transfers its phosphoryl group to the response regulator CheY and the methylesterase CheB, yielding CheY-P and CheB-P, respectively [13].

CheY-P binds to the base of the flagellar motor, increasing the probability of motor rotating clockwise (CW), namely motor CW bias, and thus increasing the cell tumble frequency [14-16]. The phosphatase CheZ binds to CheY-P and accelerates its dephosphorylation. CheB-P and CheR demethylate and methylate the receptors, respectively, to accomplish robust adaptation in chemotaxis [17-21].

Conventional stimuli are sensed by *E. coli* directly or indirectly. The former suggests that the ligand can bind to the periplasmic domain of the corresponding receptor directly and modify kinase activity, such as MeAsp and serine [22,23]. The latter requires the help of binding proteins, such as maltose sensed by the Tar receptor with the help of periplasmic maltose binding protein [24], and peptides sensed by the Tap receptor with the help of peptide binding proteins [25]. However, the detailed mechanism of bacterial sensing and response to ionic stimuli, such as the chemotactic repellent, nickel ions, is not clear [26,27]. The chemotactic response of other ions also remains to be studied.

It was discovered recently that bacteria in biofilms secrete potassium into their surroundings through ion channels on the cell membrane, thereby affecting the behavior of distant free bacteria and attracting them [28,29]. However, how limited changes in potassium concentration regulate the movement of bacteria, especially after long-distance diffusion, is still unclear.

Here, we constructed a linear concentration gradient of potassium ions with a microfluidic device, and found obvious taxis to the region of high concentration for wild-type *E. coli*. To determine the origin of this taxis, we measured the response of motor speed and CW bias to a stepwise increase in potassium concentration. The motor CW bias exhibits an attractant-like response, while the motor speed remains constant, which suggests a constant proton motive force (PMF). The chemotaxis-defective strain did not respond to this stimulus. This confirmed that the CW bias response of motors resulted from the upstream chemotaxis signaling pathway. To further characterize the response of the chemotactic signal to potassium, we directly measured the response of

kinase activity to different concentrations of potassium chloride by monitoring the FRET between CheY-eYFP and CheZ-eCFP. We ruled out the possibility of osmotaxis by comparing the responses to 30 mM potassium chloride and 60 mM sucrose. The dose-response curve and step response of kinase activity to potassium suggested a sensitive sensing process and fast adaptation. Further experiments with mutants expressing Tar, Tsr or no receptor suggested that this chemotactic response may result from the increase in intracellular pH. Our findings suggest a new mechanism of chemotactic response to ionic stimuli. Employing a coarse-grained chemotaxis model with parameters extracted from our measurements, we performed stochastic simulation of *E. coli* cells in a potassium gradient generated by a biofilm producing an oscillating potassium signal, and demonstrated the delayed periodic attraction of the cells to the biofilm.

Results

Chemotaxis in a linear concentration gradient of potassium.

It has been reported that potassium ions work as a communication agent in swarms and biofilms for both *Bacillus subtilis* and *Pseudomonas aeruginosa*. A high concentration of potassium chloride (300 mM) could attract swimming cells [28,29]. To study the chemotactic response of *E. coli* to potassium, we set up a linear concentration profile of potassium chloride with a microfluidic device designed as described previously [30,31].

As shown in Fig. 1A, a five-channel diffusion device was constructed. 2% (w/v) agarose was injected into the two resistance channels through port (***b***) to block the passage of cells without influencing the diffusion of potassium. A 100 mM potassium chloride solution, prepared in the potassium-depleted motility buffer, flows through the source channel from port (***a***) to (***a'***), while potassium-depleted motility buffer flows through the sink channel from port (***c***) to (***c'***). Potassium diffuses from the source channel to the sink channel and forms a linear concentration gradient in the observation channel [30]. The wild-type strain HCB1 was sealed in the observation channel through port (***p***) with

a drop of hot agarose (2% w/v). The movements of the cells were recorded by a high-speed CMOS camera. Four movies were recorded. An example video is shown in Movie S1. We calculated the displacement of the mean cell position for each movie. The average results are plotted in Fig. 1B. The shaded area denotes SEM. We also computed the cell density profile along the *y*-axis in the observation channel at the initial time of $t = 1$ s and steady state ($t = 300$ s). As shown in Fig. 1C, the green squares and blue dots are experimental data. The error bars denote SEM. We found that the distribution of cells is exponential at steady state, similar to the results of logarithmic chemotactic sensing in a linear MeAsp gradient [32]. The red solid line denotes the exponential fit, with a fitted decay constant of 0.0085±0.0004 μm^{-1}. As reported previously [32], the fitted exponential decay constant equals v_d/v_s, where v_d and v_s denote the drift velocity and cell motility constant, respectively. For wild-type *E. coli* with $v_s = 53.2\ \mu m^2/s$ [33], we obtained a drift velocity $v_d = 0.45 \pm 0.02\ \mu m/s$.

According to our results, the wild-type strain exhibited significant movement toward the area of high concentration in a linear concentration gradient of potassium chloride, which was similar to its chemotaxis in a typical attractant concentration gradient [31,32,34,35]. Thus, *E. coli* could be attracted by potassium and perform a trend movement in a linear gradient field on the order of millimoles. We sought to further investigate the characteristics and mechanisms of this attractant-like response.

The response of the motor rotational signal to potassium.

Potassium is important for maintaining cell membrane potential, which is one of the two components of PMF. PMF is the energy source for the flagellar motor. The absolute value of the transmembrane electrical potential will decrease when the concentration of extracellular potassium increases. This may lead to a change in PMF and affect bacterial chemotaxis by directly changing the motor behavior. However, earlier studies found that a sudden change in membrane potential in *E. coli* would result in a reverse change in the transmembrane proton concentration difference, thus keeping PMF virtually constant [36].

To test whether the chemotactic response of *E. coli* to potassium resulted from possible PMF changes, we monitored the motor response of the wild-type strain (JY26-pKAF131) to a stepwise addition of 30 mM potassium chloride using a bead assay. As shown in Fig. 2A, the cell body was attached to a 0.01% poly-l-lysine-coated cover slide. A 1-μm-diameter bead was marked on the truncated filament. We used a high-speed CMOS camera to record the rotation of the bead. As shown in Fig. 2B, the typical traces of motor rotational speed (blue line) and CW bias (purple line) were calculated. The positive and negative values of speed denote CCW (counter-clockwise) and CW (clockwise) rotation, respectively. The CW bias is positively correlated with the intracellular concentration of CheY-P [37], and the rotational speed is proportional to the PMF [38]. The stimulus (30 mM KCl) was added at t =120 s and removed at t = 480 s. The average trace of 83 motors is shown in Fig. 2C. The moments of addition and removal of stimulus were shifted to t = 0, which are marked by the purple dashed line and green dashed line, respectively. The CW bias decreased upon addition of potassium chloride, and then it adapted to a higher level than the pre-stimulus value. Such over adaptation was similar to the response of CW bias to sucrose in osomotaxis [39]. However, the motor speed remained constant during this process, confirming that the PMF remained constant, which was different from the osmotaxis response of motors. The results suggested that the response of motor CW bias to potassium was not due to PMF change. We performed further experiments with the chemotaxis-defective strain (HCB901-pBES38). The average result of 22 motors exhibited no response to 30 mM potassium chloride for either CW bias or speed (Fig. 2D), especially on the time scale of the chemotactic response as seen in the wild-type cells. These results confirmed that the CW bias response of the motor to potassium resulted from the upstream chemotaxis signaling pathway.

The response of the chemotaxis signal to potassium.

To directly measure the response of the chemotaxis signal to potassium ions, we monitored the receptor kinase activity *in vivo* by monitoring the FRET between CheY-

eYFP and CheZ-eCFP.

Using the FRET setup described previously [40], we measured the chemotactic response of a cell population with the wild-type strain (HCB1288-pVS88). We measured the response of the same sample to potassium chloride at different concentrations and to 100 μM MeAsp (a typical saturated attractant for the Tar receptor in *E. coli*). As shown in Fig. 3A, potassium (blue solid line) induces a significant chemotaxis response as an attractant. Compared with 100 μM MeAsp, 30 mM KCl resulted in a larger response and faster adaptation. Moreover, the chemotaxis signal exhibits an imprecise adaptation. This is different from the over adaptation exhibited by motor CW bias. To exclude the effect of chloride ion, we quantitatively compared the response of the chemotaxis signal to 10 mM KCl and 5 mM K_2SO_4, both of which contain 10 mM potassium ion with or without chloride ion. As shown in Fig. S1, they induce similar responses. We also measured the response of the motor rotational signal to 15 mM K_2SO_4 using the bead assay and compared it with the response to 30 mM KCl (Fig. 2C). The results are shown in Fig. S2. The response of CW bias to 15 mM K_2SO_4 exhibited an attractant response, characterized by a decreased CW bias upon the addition of K_2SO_4, followed by an over-adaptation that is qualitatively similar to the response to 30 mM KCl. Thus, the chemotactic response mainly resulted from potassium ions rather than chloride ions.

Earlier studies have shown that changes in osmotic pressure caused by a change in ion concentration on the millimole scale can also lead to chemotactic responses in *E. coli* by altering the interaction between receptors [41]. Here, we obtained a similar over adaptation in the CW bias response of motors as that of osmotaxis. To determine whether the chemotactic response to potassium was due to changes in osmotic pressure, we compared the response to both 30 mM KCl and 60 mM sucrose, both of which induced the same osmotic pressure. The results are shown in Fig. 3B. In our measurements, 60 mM sucrose induced a repellent-like response, which is consistent with previous work [41], whereas 30 mM KCl induced an attractant response. Thus, the chemotactic response of *E. coli* to KCl did not result from osmotaxis. The quantitative

comparison of the three types of chemicals is shown in Fig. 3C. The response to 30 mM KCl was 1.79 ± 0.10 times as large as that to 100 μM MeAsp, while the response to 60 mM sucrose was -0.30 ± 0.05 times as large as that to 100 μM MeAsp.

Quantitative characterization of the chemotaxis response to potassium

To quantitively describe the response of receptor-kinase activity to potassium ions, we measured the dose-response curve of HCB1288-pVS88 to potassium chloride. As shown in Fig. 4A, different concentrations of KCl were added and then removed. The FRET value of the immediate response after adding each concentration of stimulus were recorded. The FRET values were normalized by the pre-stimulus FRET value. The relative kinase activity was obtained by rescaling the FRET values of 1 (the pre-stimulus value) to 0.94 (the value after adding a saturated concentration of stimulus) to the range between 1 to 0, then the relation between relative kinase activity and concentrations of KCl was obtained (Fig. 4B).

As shown in Fig. 4B, the gray circles represent experimental data for potassium. We fitted them with a Hill function (gray dashed line). The fitted Hill coefficient was 0.53 ±0.04. However, this value was revised to 0.88± 0.14 when we corrected the FRET responses for the pH effects on the brightness of eCFP and eYFP (the blue dots and red solid line). The concentration for half-maximal response ($K_{0.5}$) was 0.64±0.12 mM before correction and 0.33 ± 0.06 mM after correction. To study the adaptation kinetics, we measured the step response for different concentrations of potassium. As shown in Fig. 4C, we calculated the adaptation percentage $P = (R^* - R_L)/(1 - R_L)$ and adaptation time T, where R^* and R_L are the adapted value and the lowest value of the FRET signal after stepwise addition of potassium, respectively. The adaptation percentage (P) and the adaptation time (T) for different concentrations of potassium are shown in Fig. 4D.

According to our measurements, *E. coli* responds sensitively (with a small $K_{0.5}$) and

adapts quickly to potassium chloride in a range of 0.01 mM-100 mM. The recovery of the chemotactic response was imprecise for all concentrations of potassium ions.

The chemotactic response to potassium may result from the intracellular pH increase.

We showed that the attractant-like response of the chemotaxis signal to potassium does not result from osmotaxis. Moreover, the PMF or motor speed did not change during that process. Considering that the absolute value of the transmembrane potential deceases as the concentration of extracellular potassium ions increases, the intracellular pH will increase to maintain a constant PMF. To confirm this, we monitored the intracellular pH using the pH-sensitive fluorescent protein pHlourin2, by computing the ratio of emitted fluorescence intensities with 405 nm and 488 nm excitations (the ratio increases with pH value) [42]. The results are shown in Fig. 5A. The intracellular pH of the wild-type strain (HCB33-pTrc99a_pHlourin2) increases immediately upon addition of 30 mM KCl. The purple arrows denote the moment of adding stimulus, while green arrows denote the moment of removing stimulus. As a control, 20 mM sodium benzoate with pH=4.55 was added at t = 720 s to decrease the intracellular pH to 4.55 [43].

It was reported that Tar and Tsr mediate opposite responses to the changes in intracellular pH [44,45]. Therefore, we measured the chemotaxis response of strains expressing only the Tar or Tsr receptor via the FRET assay. As shown in Fig. 5B, four different concentrations of KCl were added and removed successively, and the kinases activity of the Tsr-only strain exhibited an attractant response. Its imprecise adaptation is apparent as the potassium concentration increases. In contrast, the Tar-only strain exhibited a biphasic response, with kinase activity increasing sharply and then decreasing rapidly below the prestimulus level upon addition of potassium (Fig. 5C). Such a biphasic response was also observed in the response of the Tar-only strain to 40 mM sodium benzoate at pH of 7.0 (Fig. S3). Note that the cytoplasmic pH deceases upon addition of sodium benzoate at pH of 7.0, so that the response to addition of sodium benzoate is opposite to the response to addition of potassium for the Tar-only

strain. Therefore, the different responses of the Tar- and Tsr-only strains to potassium were consistent with the responses to the increase in intracellular pH.

We noted that both major receptors exhibited imprecise adaptation to stepwise addition of potassium. To investigate whether this was due to chemotactic sensing, we monitored the response of the strain with no chemoreceptors to stepwise addition of potassium. Upon addition of potassium, the FRET value decreased and remained at a constant value similar to the adapted level for the strains with chemoreceptors (Fig. 5D). This indicated that the imprecise adaptation seen for the wild-type, Tar-only and Tsr-only strains was not due to chemosensing. As the solution pH affects the brightness of fluorescent proteins, we hypothesize that this apparent imprecise adaptation was due to the differential change in eCFP and eYFP brightness when the cytoplasmic pH changed. To test this hypothesis, we bleached the eYFPs of the no-receptor strain (HCB1414-pVS88), eliminating possible FRET between CheY-eYFP and CheZ-eCFP, and compared the response of CFP fluorescence intensity to 30 mM KCl before and after bleaching. As shown in Fig. S4A, the CFP intensity showed similar amount of increase upon addition of KCl (i.e., increase of cytoplasmic pH) before and after YFP bleaching. Thus, such a response did not result from FRET, but from changes in fluorescence intensity due to an increase in intracellular pH. We calculated the ratio of CFP fluorescence intensity $P = F_r/F_b = 1.056$ without FRET, where F_r and F_b were the CFP intensity for cells in 30 mM KCl and motility medium, respectively. From this ratio we could calculate the theoretical enhancement in CFP intensity due to pH increase for the wild-type strain (HCB1288-pVS88) after adding 30 mM KCl (red dashed line in Fig. S4B), which we found was similar to the adapted level of the CFP signal. This further proved that the apparent imprecise adaptation in the FRET signal was due to changes in eCFP and eYFP brightness when the cytoplasmic pH changed.

Revised FRET responses by correcting the pH effects on the brightness of eCFP and eYFP

To minimize the impact of pH-changes altering the fluorescent protein brightness on

FRET measurements of chemotactic response and adaptation to potassium, we measured the full potassium response curve for the no-receptor mutant (HCB1414-pVS88), as shown in Fig. S5. We characterized the pH effects on CFP and YFP channels at different concentrations of KCl, and the relationship between the ratio of the signal post- to pre-KCl addition and the KCl concentration was established for both channels, as shown in Fig. S5C. The pH-corrected signal after KCl addition for strains with receptors was obtained by dividing the original signal after KCl addition by this ratio at the specific KCl concentration. This procedure was applied to both CFP and YFP channels. The pH-corrected responses for the Tar-only and Tsr-only strains are represented by red dots in Fig. 5BC.

We recalculated the FRET responses to stepwise addition of KCl, with an example depicted by the red dots in Fig. 3A. The corrected response magnitude to 30 mM KCl is similar to that of 100 μM MeAsp, being 1.06 ± 0.10 times as large, as shown by the red bar in Fig. 3C. We also calculated the dose-response curve and the adaptation curve from the pH-corrected signals, as shown in Fig. 4. The FRET signal also exhibits over-adaptation, similar to the bead assay, when we recalculated the response by correcting the CFP and YFP channels. The fitted Hill coefficient for the dose-response curve is 0.88 ± 0.14 (mean ± SD), which is close to the response to MeAsp (~1.2) [46], and the concentration for half-maximal response ($K_{0.5}$) was 0.33 ± 0.06 mM (mean ± SD).

Our results indicated that the increase in the extracellular concentration of potassium leads to an increase in the intracellular pH. The Tar and Tsr receptors respond to the increase in intracellular pH differently. The wild-type strain exhibits a similar response to the Tsr-only strain due to the larger amount of Tsr than Tar receptors. These responses could be adapted via methylation and demethylation of receptors.

The chemotaxis-based simulation of *E. coli* attraction by the potassium signal produced by a biofilm.

Based on the mechanism of potassium sensing we established here, we sought to

simulate the chemotactic swimming of *E. coli* cells in response to a periodic potassium signal secreted from a typical biofilm [28].

To simulate the periodically fluctuating field of potassium concentration produced by the biofilm, an oscillating source was introduced using a cosine function $L_s = L_0(1 - \cos(2\pi t/T))$ at position $x = 0$, where L_0 is the half maximum concentration of potassium, and T denotes the period of oscillation. In a semi-infinite liquid environment, this source results in an oscillating spatiotemporal profile of potassium

$$L(x,t) = L_0\left[1 - \cos\left(\frac{2\pi t}{T} - \sqrt{\frac{\pi}{DT}}x\right)\exp\left(-\sqrt{\frac{\pi}{DT}}x\right)\right], \qquad (1)$$

where $D = 1333.3\ \mu\mathrm{m}^2/\mathrm{s}$ is the diffusion constant of potassium in water [47]. The profile is shown in Fig. 6A (see Supplementary Material for the detailed derivation).

Similar to the two-state model of pH taxis of *E. coli* [48,49], we employed a coarse-grained model of the chemotaxis signaling pathway to simulate the chemotactic motion of *E. coli* in the potassium profile (see Materials and Methods for details) [30,31]. We utilized the Monod-Wyman-Changeux allosteric model[50] to describe the potassium sensing by chemoreceptors [51]:

$$a = \frac{1}{1 + \exp\left[N\left(f_m(m) + f_L(L)\right)\right]}, \qquad (2)$$

where a is the kinase activity of the cluster of chemoreceptors, m is the methylation level of receptors, L denotes the concentration of extracellular potassium, N is the number of receptor homodimers in an allosteric cluster, and f_m and f_L represent the methylation-dependent and ligand-dependent free energy, respectively.

$$f_L(L) = \ln\frac{1 + L/K_{off}}{1 + L/K_{on}},$$
$$f_m(m) = \alpha(m - m_0),$$

where K_{off} and K_{on} are the ligand dissociation constants for inactive and active receptors, respectively, α is the free energy change per added methyl group, and m_0 is the methylation level where f_m crosses zero. As shown in Fig. 6B, the dose-response of

kinase activity to potassium could be well fitted by Eq. 2 to extract the parameters.

In our simulation, cells swim in a square space with dimensions of $0 \leq x \leq 1500$ μm and $0 \leq y \leq 1500$ μm with a constant speed of 25 μm/s. Ten thousand cells were uniformly distributed in the space at $t = 0$. Each simulation was performed for at least four periods. An example of the traces of the mean positions in the *x*-direction (blue solid line) and *y*-direction (green solid line) is shown in Fig. 6C. The cells effectively tracked the potassium gradient and their positions exhibited fluctuations in the direction of the gradient, similar to that observed experimentally by Humphries *et al* [28]. Furthermore, a phase delay between the mean *x*-position and the potassium source was observed, indicating a temporal shift in response.

We simulated the taxis of cells under the oscillating source with $L_0 = 1$ mM and T =1, 2, 3 and 4 hours. Four typical traces are shown in Fig. 6D, and the relation between the phase shift ($\Delta\phi$, as denoted in Fig. 6C) and the driving period (T) is shown in Fig. 6E. We found that the phase delay decreases significantly with the increase of driving period, a trend that is consistent with previous experimental observations in the biofilm [28]. Similar behavior was observed in frequency-dependent *E. coli* chemotaxis to spatially and temporally varying MeAsp source [52]. Furthermore, we also computed the lag time ($\Delta\phi \cdot T$) of the average *x* position relative to the electric signal (potassium concentration). The relation between lag time and the driving period is shown in Fig. 6F. For driving periods of 1, 2, 3 and 4 hours, the oscillation in the *E. coli* cell displacement lagged the potassium source by 11.7±0.5, 14.7±0.7, 14.8±0.9 and 14.2± 1.0 min (mean±SD), respectively. These values closely resemble the 9 to 35-min lag observed in biofilm experiments for *Bacillus subtilis* and *Pseudomonas aeruginosa* [28]. Notably, this result was not affected by the specific value of L_0 (Fig. S6).

Discussion

Potassium ions play a critical role in many physiological processes of bacteria. Bacteria

in biofilms release potassium ions to their surroundings through ion channels on the cell membrane, thus influencing the behavior of surrounding bacteria and attracting distant free bacteria to swim toward them. However, the mechanism of bacterial sensing and response to potassium ions was unclear. Here, we found that *E. coli* senses the concentration change of extracellular potassium ions sensitively via the chemotaxis signaling pathway, and this chemotactic sensing is achieved through changes in intracellular pH.

We found that *E. coli* could quickly converge to the area with a higher concentration of potassium under a linear concentration profile. The measurements of the response of individual motors to stepwise addition and removal of 30 mM KCl via the bead assay demonstrated that the attractant response resulted from the chemotaxis signaling pathway instead of the possible PMF effect on the motor itself. We also demonstrated that the PMF remained unchanged when KCl was added or removed.

To directly measure the chemotactic response of *E. coli* to potassium ions, we measured the response to different concentrations of potassium via FRET between CheY-eYFP and CheZ-eCFP. After correcting the pH effects on the brightness of CFP and YFP proteins, we found that the chemotactic response of wild-type *E. coli* to 30 mM KCl was 1.06 ± 0.10 times that to 100 μM MeAsp. The response to 60 mM sucrose was -0.30 ± 0.05 times that to 100 μM MeAsp. This suggested that the attractant response to potassium was independent of the osmolality response. To quantitatively describe the chemotactic response to potassium, we systematically measured the dose-response curve and the step responses. We obtained a Hill coefficient of 0.88±0.14 and a concentration of 0.33±0.06 mM for the half-maximal response. This showed that *E. coli* had a very sensitive response to potassium ions and could sense weak changes in potassium concentration. We also found that *E. coli* adapts quickly to potassium concentration changes in the range of 0.01 mM-100 mM, which promotes cell localization to the peak of a potassium concentration profile.

For other strong attractant stimuli such as high concentrations of MeAsp, the step response typically shows a low plateau before it adapts. However, in the case of potassium, the FRET signal does not typically display an obvious plateau following the stimuli. To observe the low plateau before adaptation, a saturating amount of attractant should be added in a stepwise manner. According to the dose-response curve we measured for potassium, a saturating amount of potassium would be close to 100 mM. In fact, there is a small segment of the low plateau in the step response to 30 mM KCl (Fig. 4C). To observe more of this low plateau, we could have used a higher concentration of KCl. However, a stimulation higher than 30 mM KCl will induce substantial physiological changes in the cell, resulting in a significant decrease in fluorescence for both channels (Fig. S7). Therefore, the range of KCl concentration that can be reliably applied in FRET measurements is limited.

While keeping the PMF unchanged, addition of potassium decreases the membrane potential and thus increases the intracellular pH. This was demonstrated by intracellular pH measurements. We also measured the chemotaxis response of mutant strains expressing only Tsr or Tar to different concentrations of potassium. The Tsr-only strain responded to potassium as an attractant, whereas the Tar-only strain exhibited a biphasic response (a repellent-like followed by an attractant-like response). The different responses of Tar and Tsr to potassium were consist with their responses to changes in intracellular pH. We further demonstrated the biphasic response of the Tar-only strain to 40 mM sodium benzoate with pH of 7.0 that induced a decrease in intracellular pH. The differential responses of the Tsr and Tar receptors to potassium may be a strategy by which bacteria adjust their response to potassium at different growth stages during which bacteria express different ratios of Tsr to Tar receptors [53,54]. For the growth stage used in our measurements here, the amount of Tsr was more than that of Tar in the wild-type strain [55], so the response to potassium was dominated by Tsr.

The response of the Tar-only strain to potassium warrants further discussion (Fig. 5C). This strain shows a repellent response to stepwise addition of low concentrations of

potassium, specifically less than 10 mM. This is consistent with previous observations of the response of Tar to changes in intracellular pH [44,45]. Interestingly, it exhibits a biphasic response to high potassium concentrations of 10 mM and above. This biphasic response might result from additional pH-effects on the activity of intracellular enzymes such as CheRB and CheA [56], which may have a different timescale and response from the Tar receptor.

Based on the potassium sensing mechanism we established here, we performed stochastic simulation of bacterial taxis in a biofilm-produced potassium gradient, demonstrating that *E. coli* cells can be periodically attracted by the biofilm. Moreover, we observed a time delay between the positions of the cells and the electric signal of the biofilm. Specifically, we found that the oscillation of *E. coli* cell displacement lags the potassium source by 11.7±0.5 min, 14.7±0.7 min, 14.8±0.9 min and 14.2±1.0 min (mean±SD) for driving periods of 1, 2, 3 and 4 hours, respectively. Remarkably, these values closely resemble the 9 to 35-min lag observed in biofilm experiments for *Bacillus subtilis* and *Pseudomonas aeruginosa* [28], despite the potential variations in the potassium sensing mechanisms among these bacterial species. The potassium sensing mechanism we established here contributed to our understanding of the complex dynamics of electrical signaling in biofilm environments.

Materials and methods

Strains and plasmids

Strain HCB1 was derived from *E. coli* K12 strain AW405. Strains JY26 (Δ*filC*), HCB33, HCB901 (Δ*cheZ fliC*, Ptrc420 $cheY^{13DK106YW}$), HCB1288 (Δ*cheY cheZ*), and HCB1414 (Δ*tar tsr tap trg aer cheY cheZ*) were derived from *E. coli* K12 strain RP437. The plasmid pKAF131 constitutively expresses $FliC^{sticky}$. The plasmid pBES38 constitutively expresses both $LacI^{q}$ and the sticky filament $FliC^{sticky}$. The promoters used for the constitutive expression of $LacI^{q}$ and $FliC^{sticky}$ were the I^{q} promotor and the

native promoter of *fliC*, respectively [57]. The FRET pair CheY-eYFP and CheZ-eCFP was expressed from plasmid pVS88 under an isopropyl-β-d-thiogalactoside (IPTG)-inducible promoter. The plasmid pVS18 was used to express CheY-eYFP under an IPTG-inducible promoter. The plasmids pLC113 and pPA114 were used to express Tar and Tsr receptors under a salicylate-inducible promoter, respectively. The gene *pHluorin2* was cloned into pTrc99a under an IPTG-inducible promoter, yielding pTrc99a_pHluorin2. The strains and plasmids used in this study are shown in Table 1.

Table 1 Strains and plasmids used in this study

Strain	Plasmids	Assay
HCB1	-	Microfluidic assay
JY26	pKAF131	Bead assay
HCB901	pBES38	Bead assay
HCB1288	pVS88	FRET assay
	pVS18	FRET assay
HCB1414	pVS88	FRET assay
	pLC113, pVS88	FRET assay
	pPA114, pVS88	FRET assay
HCB33	pTrc99a_pHluorin2	Intracellular pH measurement

Cell culture

All cells were grown at 33 °C in 10 ml T-broth (1% tryptone and 0.5% NaCl) to an OD_{600} between 0.45-0.50 with appropriate antibiotics and inducers, collected by centrifugation and washed twice with potassium-depleted motility buffer (10 mM $NaPO_4$, 0.1 mM EDTA, 1 mM methionine, 10 mM lactate, pH 7.0). Cells of HCB1 were centrifuged for 6 min at 1200 ×g. Cells of JY26-pKAF131 were grown with 25 μg/ml chloramphenicol. HCB901-pBES38 cells were grown with 100 μg/ml ampicillin and 23 μM IPTG. Both were centrifuged for 2 min at 4000 ×g. Cells of HCB1288-pVS88 and HCB1414-pVS88 were grown with 100 μg/ml ampicillin and 100 μM IPTG in the dark. Cells of HCB1414-pLC113-pVS88 and HCB1414-pPA114-pVS88 were grown with 100 μg/ml ampicillin, 25 μg/ml chloramphenicol, 100 μM IPTG and 1 μM

salicylate in the dark. Cells of HCB33-pTrc99a_pHlourin2 were grown with 100 μg/ml ampicillin and 100 μM IPTG. Cells were stored at 4 °C before use. All experiments were carried out at 23 °C. The KCl solution used in this work was prepared in the potassium-depleted motility buffer.

Microfluidics

We constructed a 100-μm-depth microfluidic device similar to that described previously [30,31]. The design is shown in Fig. 1A. There are two auxiliary channels and three primary channels. The width of the auxiliary channels is 100 μm, while the width of the primary channels is 400 μm. The source and sink channels were used to flow 100 mM KCl and potassium-depleted motility buffer, respectively, and the observing channel was used to observe the motion of cells. The auxiliary channels were filled with 2% agarose gel at a temperature of 68°C and cooled down. In our measurement, we kept the flow at a rate of 5 ml/min in both source and sink channels with a syringe pump (Pump-22; Harvard Apparatus). The potassium ions could diffuse from the source channel to the sink channel and form a linear gradient in the observing channel. Cells of HCB1 were sealed in the observing channel, and their movement was recorded by a fast CMOS camera (Flare 2M360-CL, IO Industries) equipped on a Nikon Ti-E microscope at a magnification of 20×. The chemotaxis migration coefficient (CMC), as an indicator of the mean cell position (49), was calculated as the average of $(x_i - x_c)/194$, where x_i is the x-position of the ith cell, x_c is the x-position of the center of the observing channel, and 194 μm is the half-width of the observed region.

Bead assay

We sheared the sticky filaments of the washed cell suspensions by passing them 200 times between two syringes equipped with 23-gauge needles and connected by a 7-cm-long polyethylene tube (0.58 mm inside diameter, no.0427411; Becton Dickinson), and condensed them into 300 μl in potassium-depleted motility buffer. To measure motor rotation, sheared cells were immobilized on a coverslip coated with poly-L-lysine (0.01%, P4707; Sigma, St. Louis, MO) assembled on a flow chamber [58], and allowed

to stand for 5 min. Then, 1-μm-diameter polystyrene beads (0.27%, no. 0731; Polysciences) were flowed to replace the suspension and attached to the sheared filament stubs by allowing it to stand for 4 min. The rotation of beads was recorded by a fast CMOS camera (Flare 2M360-CL, IO Industries) equipped on a Nikon Ti-E inverted phase-contrast microscope at a magnification of 40×. The CW bias and rotational speed were calculated with a 20-s time window and 1-s time slide.

FRET assay

The experimental setup used in FRET measurements was the same as that described previously [40]. The FRET setup was based on a Nikon Ti-E microscope equipped with a 40× 0.60 NA objective. The illumination light was provided by a 130-W mercury lamp, attenuated by a factor of 1024 with neutral density filters, and passed through an excitation bandpass filter (FF02-438/24-25, Semrock) and a dichroic mirror (FF458-Di02-25x36, Semrock). The epifluorescent emission was split into cyan and yellow channels by a second dichroic mirror (FF509-FDi01-25x36, Semrock). The signals in the two channels were then filtered by two emission bandpass filters (FF01-483/32-25 and FF01-542/32-25, Semrock) and collected by two photon-counting photomultipliers (H7421-40, Hamamatsu, Hamamatsu City, Japan), respectively. Signals from the two photomultipliers were recorded at a sampling rate of 1 Hz using a data-acquisition card installed in a computer (USB-1901(G)-1020, ADlink, New Taipei, Taiwan).

The washed cell suspension was concentrated 45 times and flowed into a flow chamber equipped with a poly-L-lysine-coated coverslip, allowing it to stand for 20 min. Then, the chamber was maintained under a constant flow (500 μl/min) of potassium-depleted motility buffer by a syringe pump (Pump-22; Harvard Apparatus). The same flow was used to add and remove stimulus. All data analysis was performed using custom scripts in MATLAB 2018b (MathWorks). The FRET value was calculated as the ratio of YFP to CFP intensities, normalized by the prestimulus value. The impact of pH on the original signals for both CFP and YFP channels was corrected by

$$S_{pH-corrected}(L; t_{addition} < t < t_{removal}) = \frac{S_{orignal}(L; t_{addition} < t < t_{removal})}{C_{pH}(L)}$$

where $S_{pH-corrected}(L; t_{addition} < t < t_{removal})$ and $S_{orignal}(L; t_{addition} < t < t_{removal})$ represent the pH-corrected and original PMT signal (CFP or YFP channel) from the moment of addition of L mM KCl to the moment of its removal, respectively, and $C_{pH}(L)$ is the correction factor, which is the ratio of PMT signal post- to pre-KCl addition for the no-receptor mutant at L mM KCl, for CFP or YFP channel as shown Fig. S5. The pH-corrected FRET response is then calculated as the ratio of the pH-corrected YFP to the pH-corrected CFP, normalized by the pre-stimulus ratio.

For the YFP photobleaching assay, we measured the background of the CFP channel by recording the intensity of the CFP channel for the strain expressing only CheY-eYFP (HCB1288-pVS18). We monitored the response of the CFP signal to 30 mM KCl before and after bleaching YFP. The bleaching was carried out with a YFP filter set (C-FL YFP BP HYQ535, #41028, Chroma) under mercury lamp illumination without attenuation and sustained for 50 minutes. All these measurements were performed under the same conditions.

Intracellular pH measurements

The washed cells of HCB33-pTrc99a_pHluorin2 were immobilized on a coverslip assembled on a flow chamber and coated with poly-L-lysine. Then, a constant flow (500 μl/min) was applied to the cells. The samples were illuminated periodically with two lasers. In each period, the laser with a wavelength of 405 nm was illuminated for 200 ms and stopped for 400 ms, and the laser with a wavelength of 488 nm was illuminated for another 200 ms and stopped for another 400 ms. The emission light passed through the T495lp dichroic mirror and AT495lp longpass filter and was collected by an EMCCD (Andor DU897) equipped on a Nikon Ti-E inverted phase-contrast microscope at a magnification of 100×. The changes in intracellular pH could be characterized by the ratio of emitted fluorescence between the two excitation lasers.

Simulation of bacterial taxis in an oscillating spatial gradient of potassium.

In our simulation, cells were treated as self-propelled particles. They could swim smoothly (a run state) with a constant speed of 25 μm/s and with rotational diffusion (the rotational diffusion constant was 0.062 rad^2/s) [59], or stop to reorient (a tumble state). The tumble angle θ was selected from the probability distribution $P(\theta) = 0.5 * (1 + \cos\theta) * \sin\theta \ (0 \leq \theta \leq \pi)$.[22,60] A coarse-grained model of the chemotaxis signaling pathway[34,51] was utilized to describe the sensing and adaptation of chemoreceptors to changes in extracellular potassium concentration:

$$a = \frac{1}{1 + \exp\left[N\left(\alpha(m - m_0) + \ln\frac{1 + L/K_{off}}{1 + L/K_{on}}\right)\right]}, \quad (3)$$

$$\frac{dm}{dt} = k_R(1 - a) - k_B a, \quad (4)$$

where a is the kinase activity of the cluster of chemoreceptors, m is the methylation level of receptors, and L denotes the concentration of extracellular potassium. In the denominator on the right-hand side of Eq. 3, the two terms within the parentheses of the exponential expression represent the methylation-dependent (f_m) and ligand-dependent (f_L) free energy, respectively. The parameters $N = 0.85$, $f_m = 0.84$, $K_{off} = 0.17$ mM, $K_{on} = 55.17$ mM were determined by fitting the dose-response curve in Fig. 6B. The values of the parameters $\alpha = -1.7, m_0 = 1.0, k_R = 0.005\ s^{-1}, k_B = 0.010\ s^{-1}$ were chosen to be the same as before[31].

The CheY-P concentration (Yp) is proportional to the kinase activity: $Yp = 7.86a$ [34,61], and is related to the motor CW bias (B) by [62]

$$B = \frac{Yp^{10.3}}{Yp^{10.3} + 3.1^{10.3}}. \quad (5)$$

Then the switching rate from run to tumble and from tumble to run were determined by $B/0.11\ s^{-1}$ and $5\ s^{-1}$, respectively [60,63].

In the simulation, cells swim in a square space with dimensions of $0 \leq x \leq 1500$ μm and $0 \leq y \leq 1500$ μm. We implemented periodic boundary condition for the y direction, and reflective boundaries for the x direction. Ten thousand cells were uniformly distributed throughout the square space at $t = 0$. The time step is 0.01 s.

They swam in a steady oscillating spatial gradient of potassium created by an oscillating source at $x = 0$. The simulation was performed for a minimum of four periods to observe and analyze the long-term behavior of the cells in response to the oscillating gradient. The simulated lag time decreases with the methylation rate k_R, but levels off at high values of k_R (Fig. S8).

References

1 Gründling, A. Potassium Uptake Systems in Staphylococcus aureus: New Stories about Ancient Systems. *mBio* **4**, e00784-00713, doi:10.1128/mBio.00784-13 (2013).

2 Zacchia, M., Abategiovanni, M. L., Stratigis, S. & Capasso, G. Potassium: From Physiology to Clinical Implications. *KIDNEY DIS-BASEL* **2**, 72-79, doi:10.1159/000446268 (2016).

3 Li, S. *et al.* Cryo-EM structure of the hyperpolarization-activated inwardly rectifying potassium channel KAT1 from Arabidopsis. *Cell Res.* **30**, 1049-1052, doi:10.1038/s41422-020-00407-3 (2020).

4 Ballal, A., Basu, B. & Apte, S. K. The Kdp-ATPase system and its regulation. *J. Biosci.* **32**, 559-568, doi:10.1007/s12038-007-0055-7 (2007).

5 Epstein, W. The roles and regulation of potassium in bacteria. *Prog Nucleic Acid Res Mol Biol* **75**, 293-320, doi:10.1016/s0079-6603(03)75008-9 (2003).

6 Nanatani, K. *et al.* Comparative Analysis of *kdp* and *ktr* Mutants Reveals Distinct Roles of the Potassium Transporters in the Model Cyanobacterium Synechocystis sp. Strain PCC 6803. *J. Bacteriol.* **197**, 676-687, doi:10.1128/JB.02276-14 (2015).

7 Ali, M. K. *et al.* Regulation of Inducible Potassium Transporter KdpFABC by the KdpD/KdpE Two-Component System in Mycobacterium smegmatis. *Front. Microbiol.* **8**, doi:10.3389/fmicb.2017.00570 (2017).

8 Bray, D., Levin, M. D. & Morton-Firth, C. J. Receptor clustering as a cellular mechanism to control sensitivity. *Nature* **393**, 85-88, doi:10.1038/30018 (1998).

9 Endres, R. G. *et al.* Variable sizes of Escherichia coli chemoreceptor signaling teams. *Mol Syst Biol* **4**, 211, doi:10.1038/msb.2008.49 (2008).

10 Homma, M., Shiomi, D., Homma, M. & Kawagishi, I. Attractant binding alters arrangement of chemoreceptor dimers within its cluster at a cell pole. *Proc Natl Acad Sci U S A* **101**, 3462-3467, doi:10.1073/pnas.0306660101 (2004).

11 Li, M. & Hazelbauer, G. L. Core unit of chemotaxis signaling complexes. *Proc Natl Acad Sci U S A* **108**, 9390-9395, doi:10.1073/pnas.1104824108 (2011).

12 Li, X. *et al.* The 3.2 Å Resolution Structure of a Receptor:CheA:CheW Signaling Complex Defines Overlapping Binding Sites and Key Residue Interactions within Bacterial Chemosensory Arrays. *Biochemistry* **52**,

doi:10.1021/bi400383e (2013).
13 Bren, A. & Eisenbach, M. How signals are heard during bacterial chemotaxis: protein-protein interactions in sensory signal propagation. *J. Bacteriol.* **182**, 6865-6873, doi:10.1128/jb.182.24.6865-6873.2000 (2000).
14 Dyer, C. M. & Dahlquist, F. W. Switched or not?: the structure of unphosphorylated CheY bound to the N terminus of FliM. *J. Bacteriol.* **188**, 7354-7363, doi:10.1128/jb.00637-06 (2006).
15 Lam, K. H. *et al.* Structural basis of FliG-FliM interaction in Helicobacter pylori. *Mol. Microbiol.* **88**, 798-812, doi:10.1111/mmi.12222 (2013).
16 van Albada, S. B. & Ten Wolde, P. R. Differential affinity and catalytic activity of CheZ in E. coli chemotaxis. *PLoS Comput Biol* **5**, e1000378, doi:10.1371/journal.pcbi.1000378 (2009).
17 Djordjevic, S. & Stock, A. M. Chemotaxis receptor recognition by protein methyltransferase CheR. *Nat Struct Biol* **5**, 446-450, doi:10.1038/nsb0698-446 (1998).
18 Levin, M. D., Shimizu, T. S. & Bray, D. Binding and diffusion of CheR molecules within a cluster of membrane receptors. *Biophys. J.* **82**, 1809-1817, doi:10.1016/s0006-3495(02)75531-8 (2002).
19 Lupas, A. & Stock, J. Phosphorylation of an N-terminal regulatory domain activates the CheB methylesterase in bacterial chemotaxis. *J Biol Chem* **264**, 17337-17342 (1989).
20 Lybarger, S. R. & Maddock, J. R. Clustering of the chemoreceptor complex in Escherichia coli is independent of the methyltransferase CheR and the methylesterase CheB. *J. Bacteriol.* **181**, 5527-5529, doi:10.1128/jb.181.17.5527-5529.1999 (1999).
21 Djordjevic, S. & Stock, A. M. Crystal structure of the chemotaxis receptor methyltransferase CheR suggests a conserved structural motif for binding S-adenosylmethionine. *Structure* **5**, 545-558, doi:10.1016/s0969-2126(97)00210-4 (1997).
22 Neumann, S., Hansen, C. H., Wingreen, N. S. & Sourjik, V. Differences in signalling by directly and indirectly binding ligands in bacterial chemotaxis. *EMBO J.* **29**, 3484-3495, doi:10.1038/emboj.2010.224 (2010).
23 Tajima, H. *et al.* Ligand specificity determined by differentially arranged common ligand-binding residues in bacterial amino acid chemoreceptors Tsr and Tar. *J Biol Chem* **286**, 42200-42210, doi:10.1074/jbc.M111.221887 (2011).
24 Brass, J. M. & Manson, M. D. Reconstitution of maltose chemotaxis in Escherichia coli by addition of maltose-binding protein to calcium-treated cells of maltose regulon mutants. *J. Bacteriol.* **157**, 881-890, doi:10.1128/jb.157.3.881-890.1984 (1984).
25 Manson, M. D., Blank, V., Brade, G. & Higgins, C. F. Peptide chemotaxis in E. coli involves the Tap signal transducer and the dipeptide permease. *Nature* **321**, 253-256, doi:10.1038/321253a0 (1986).
26 de Pina, K. *et al.* Purification and characterization of the periplasmic nickel-binding protein NikA of Escherichia coli K12. *Eur J Biochem* **227**, 857-865,

doi:10.1111/j.1432-1033.1995.tb20211.x (1995).
27 Englert, D. L., Adase, C. A., Jayaraman, A. & Manson, M. D. Repellent taxis in response to nickel ion requires neither Ni2+ transport nor the periplasmic NikA binding protein. *J. Bacteriol.* **192**, 2633-2637, doi:10.1128/jb.00854-09 (2010).
28 Humphries, J. *et al.* Species-Independent Attraction to Biofilms through Electrical Signaling. *Cell* **168**, 200-209 e212, doi:10.1016/j.cell.2016.12.014 (2017).
29 Prindle, A. *et al.* Ion channels enable electrical communication in bacterial communities. *Nature* **527**, 59-63, doi:10.1038/nature15709 (2015).
30 Tian, M., Zhang, C., Zhang, R. & Yuan, J. Collective motion enhances chemotaxis in a two-dimensional bacterial swarm. *Biophys. J.* **120**, 1615-1624, doi:10.1016/j.bpj.2021.02.021 (2021).
31 Liu, X., Zhang, C., Zhang, R. & Yuan, J. The Effect of the Second Messenger c-di-GMP on Bacterial Chemotaxis in Escherichia coli. *Appl. Environ. Microbiol.* **88**, e00373-00322, doi:doi:10.1128/aem.00373-22 (2022).
32 Kalinin, Y. V., Jiang, L., Tu, Y. & Wu, M. Logarithmic Sensing in Escherichia coli Bacterial Chemotaxis. *Biophys. J.* **96**, 2439-2448, doi:10.1016/j.bpj.2008.10.027 (2009).
33 Wu, M., Roberts, J. W., Kim, S., Koch, D. L. & DeLisa, M. P. Collective Bacterial Dynamics Revealed Using a Three-Dimensional Population-Scale Defocused Particle Tracking Technique. *Appl. Environ. Microbiol.* **72**, 4987-4994, doi:10.1128/AEM.00158-06 (2006).
34 Jiang, L., Ouyang, Q. & Tu, Y. Quantitative Modeling of *Escherichia coli* Chemotactic Motion in Environments Varying in Space and Time. *PLoS Comput. Biol.* **6**, e1000735 (2010).
35 Son, K., Menolascina, F. & Stocker, R. Speed-dependent chemotactic precision in marine bacteria. *Proc Natl Acad Sci U S A* **113**, 8624-8629, doi:10.1073/pnas.1602307113 (2016).
36 Bakker, E. P. & Mangerich, W. E. Interconversion of components of the bacterial proton motive force by electrogenic potassium transport. *J. Bacteriol.* **147**, 820-826, doi:10.1128/jb.147.3.820-826.1981 (1981).
37 Cluzel, P., Surette, M. & Leibler, S. An ultrasensitive bacterial motor revealed by monitoring signaling proteins in single cells. *Science* **287**, 1652-1655, doi:10.1126/science.287.5458.1652 (2000).
38 Gabel, C. & Berg, H. The speed of the flagellar rotary motor of Escherichia coli varies linearly with protonmotive force. *Proc Natl Acad Sci U S A* **100**, 8748-8751, doi:10.1073/pnas.1533395100 (2003).
39 Rosko, J., Martinez, V. A., Poon, W. C. K. & Pilizota, T. Osmotaxis in Escherichia coli through changes in motor speed. *Proc Natl Acad Sci U S A* **114**, E7969-e7976, doi:10.1073/pnas.1620945114 (2017).
40 Zhang, C., He, R., Zhang, R. & Yuan, J. Motor Adaptive Remodeling Speeds Up Bacterial Chemotactic Adaptation. *Biophys. J.* **114**, 1225-1231, doi:10.1016/j.bpj.2018.01.018 (2018).
41 Vaknin, A. & Berg, H. C. Osmotic stress mechanically perturbs chemoreceptors

in *Escherichia coli*. *Proc Natl Acad Sci U S A* **103**, 592-596, doi:10.1073/pnas.0510047103 (2006).

42 Mahon, M. J. pHluorin2: an enhanced, ratiometric, pH-sensitive green florescent protein. *Adv Biosci Biotechnol* **2**, 132-137, doi:10.4236/abb.2011.23021 (2011).

43 Nakamura, S. *et al.* Effect of intracellular pH on the torque-speed relationship of bacterial proton-driven flagellar motor. *J. Mol. Biol.* **386**, 332-338, doi:10.1016/j.jmb.2008.12.034 (2009).

44 Krikos, A., Conley, M. P., Boyd, A., Berg, H. C. & Simon, M. I. Chimeric chemosensory transducers of Escherichia coli. *Proc Natl Acad Sci U S A* **82**, 1326-1330, doi:10.1073/pnas.82.5.1326 (1985).

45 Umemura, T., Matsumoto, Y., Ohnishi, K., Homma, M. & Kawagishi, I. Sensing of cytoplasmic pH by bacterial chemoreceptors involves the linker region that connects the membrane-spanning and the signal-modulating helices. *J Biol Chem* **277**, 1593-1598, doi:10.1074/jbc.M109930200 (2002).

46 Sourjik, V. & Berg, H. C. Receptor sensitivity in bacterial chemotaxis. *Proc Natl Acad Sci U S A* **99**, 123-127 (2002).

47 Fell, C. J. D. & Hutchison, H. P. Diffusion coefficients for sodium and potassium chlorides in water at elevated temperatures. *J. Chem. Eng. Data* **16**, 427-429, doi:10.1021/je60051a005 (1971).

48 Hu, B. & Tu, Y. Behaviors and strategies of bacterial navigation in chemical and nonchemical gradients. *PLoS Comput. Biol.* **10**, e1003672 (2014).

49 Hu, B. & Tu, Y. Precision sensing by two opposing gradient sensors: how does Escherichia coli find its preferred pH level? *Biophys. J.* **105**, 276-285 (2013).

50 Monod, J., Wyman, J. & Changeux, J.-P. On the nature of allosteric transitions: A plausible model. *J. Mol. Biol.* **12**, 88-118 (1965).

51 Tu, Y., Shimizu, T. S. & Berg, H. C. Modeling the chemotactic response of Escherichia coli to time-varying stimuli. *Proc Natl Acad Sci U S A* **105**, 14855-14860 (2008).

52 Zhu, X. *et al.* Frequency-dependent *Escherichia coli* chemotaxis behavior. *Phys. Rev. Lett.* **108**, 128101 (2012).

53 Kalinin, Y., Neumann, S., Sourjik, V. & Wu, M. Responses of *Escherichia coli* Bacteria to Two Opposing Chemoattractant Gradients Depend on the Chemoreceptor Ratio. *J. Bacteriol.* **192**, 1796-1800, doi:10.1128/JB.01507-09 (2010).

54 Yang, Y. & Sourjik, V. Opposite responses by different chemoreceptors set a tunable preference point in Escherichia coli pH taxis. *Mol. Microbiol.* **86**, 1482-1489, doi:10.1111/mmi.12070 (2012).

55 Li, M. & Hazelbauer, G. L. Cellular Stoichiometry of the Components of the Chemotaxis Signaling Complex. *J. Bacteriol.* **186**, 3687-3694, doi:10.1128/JB.186.12.3687-3694.2004 (2004).

56 Conley, M. P. *et al.* pH dependence of CheA autophosphorylation in *Escherichia coli*. *J. Bacteriol.* **176**, 3870–3877 (1994).

57 Scharf, B. E., Fahrner, K. A., Turner, L. & Berg, H. C. Control of direction of

flagellar rotation in bacterial chemotaxis. *Proc Natl Acad Sci U S A* **95**, 201–206 (1998).

58 Berg, H. C. & Block, S. M. A miniature flow cell designed for rapid exchange of media under high-power microscope objectives. *J Gen Microbiol* **130**, 2915-2920, doi:10.1099/00221287-130-11-2915 (1984).

59 Vladimirov, N., Lebiedz, D. & Sourjik, V. Predicted Auxiliary Navigation Mechanism of Peritrichously Flagellated Chemotactic Bacteria. *PLoS Comput. Biol.* **6**, e1000717, doi:10.1371/journal.pcbi.1000717 (2010).

60 Berg, H. C. & Brown, D. A. Chemotaxis in *Escherichia coli* analysed by Three-dimensional Tracking. *Nature* **239**, 500-504, doi:10.1038/239500a0 (1972).

61 van Albada, S. B. & ten Wolde, P. R. Differential Affinity and Catalytic Activity of CheZ in E. coli Chemotaxis. *PLoS Comput Biol* **5**, e1000378, doi:10.1371/journal.pcbi.1000378 (2009).

62 Cluzel, P., Surette, M. & Leibler, S. An ultrasensitive bacterial motor revealed by monitoring signaling proteins in single cells. *Science* **287**, 1652-1655 (2000).

63 He, R., Zhang, R. & Yuan, J. Noise-Induced Increase of Sensitivity in Bacterial Chemotaxis. *Biophys. J.* **111**, 430-437, doi:10.1016/j.bpj.2016.06.013 (2016).

Acknowledgements This work was supported by National Natural Science Foundation of China Grants (11925406, 12090053, and 12104436), a grant from the Ministry of Science and Technology of China (2019YFA0709303), and the Fundamental Research Funds for the Central Universities (WK2030000026).

Author Contributions J. Y., R.Z., and C. Z. designed the work, C. Z. performed the experiments and simulation. J. Y., R.Z., and C. Z. wrote the manuscript.

Competing financial interests The authors declare no competing financial interests.

Figure Legends

Fig. 1. The chemotaxis performance of *E. coli* in a linear concentration gradient of potassium. **A.** Design diagram of the microfluidic device. The source channel and sink were flowed with 100 mM KCl and motility buffer, respectively. The inlets of KCl, agarose, motility buffer and cells are denoted by (***a***), (***b***), (***c***) and (***p***), respectively. The outlets are labeled by the corresponding letters with the prime symbol. **B.** The average CMC of four datasets as a function of time for the wild-type strain (HCB1) under a linear concentration gradient of KCl. The shaded area denotes SEM. **C.** The cell density profile in the observing channel along the *y*-axis at the beginning (t = 1 s, green squares) and a steady state (t = 300 s, blue dots). The red solid line is an exponential fit to the data. Error bars denote SEM.

Fig. 2. The response of motor rotational signal to potassium. **A.** Schematic diagram of the bead assay for the flagellar motor. B. Typical trace of rotational speed (blue line) and CW bias (purple line) of individual motors for the wild-type strain (JY26-pKAF131). The positive and negative values of speed denote CCW and CW rotation, respectively. 30 mM KCl was added at t =120 s and removed at t = 480 s. **C.** The average response of 83 motors from 5 samples for the wild-type strain to 30 mM KCl. The vertical purple (green) dashed lines indicate the moment of adding (removing) stimulus. The shaded areas denote SEM. **D.** The average response of 22 motors from 4 samples for the chemotaxis-defective strain (HCB901-pBES38) to 30 mM KCl. The vertical purple (green) dashed lines indicate the moment of adding (removing) stimulus. The shaded areas denote SEM.

Fig. 3. The chemotactic response of the wild-type strain (HCB1288-pVS88) to potassium. **A.** Chemotactic response of the wild-type strain (HCB1288-pVS88) to stepwise addition and removal of KCl. The blue solid line denotes the orignal signal, and the red dots represent the pH-corrected signal, which was recalculated from the pH-corrected CFP and YFP channels using the response of the no-receptor strain. **B.**

Comparison of the chemotactic response to 30 mM KCl and 60 mM sucrose. The vertical purple (green) dashed lines indicate the moment of adding (removing) stimulus. **C.** Quantitative comparison among the responses to 100 μM MeAsp, 30 mM KCl and 60 mM sucrose. The hollow and solid red bars represent the value calculated from the original signal and the pH-corrected signal, respectively. The errors denote SEM.

Fig. 4. Quantitative results of the chemotactic response of the wild-type strain (HCB1288-pVS88) to potassium. **A.** A typical example of the dose-response measurement. The blue solid line denotes the original signal, and the red dots represent the pH-corrected signal, recalculated from the pH-corrected CFP and YFP signals using the response of the no-receptor strain. The vertical purple (green) dashed lines indicate the moment of adding (removing) stimulus. **B.** The dose-response curve of relative kinase activity to KCl. The blue dots and gray circles represent the pH-corrected and original experimental data, respectively. The red solid and gray dashed lines are the fit curves for the blue dots and gray circles, respectively, using a Hill function. The fitted Hill coefficient for original and pH-corrected response were 0.53±0.04 and 0.88±0.14, respectively, and the concentration for half-maximal response ($K_{0.5}$) were 0.64±0.12 mM and 0.33±0.06 mM, accordingly. **C.** Definition of adaptation time in the step response. The gray and blue lines represent the original and pH-corrected signals, respectively. **D.** The adaptation level $P = (\mathrm{R}^* - \mathrm{R_L})/(1 - \mathrm{R_L})$ and adaptation time (T) as a function of the concentration of KCl, calculated with pH-corrected data. The errors denote SEM.

Fig. 5. **A.** The response of intracellular pH to 30 mM KCl for the wild-type strain (HCB33-pTrc99a_pHluorin2). The response to 20 mM sodium benzoate solution with pH=4.55 was used as a control. **B.** The chemotactic response of the Tsr-only strain (HCB1414-pPA114-pVS88) to four typical concentrations of potassium. The blue line denotes the orignal signal, and the red dots represent the pH-correcting signal. **C.** The chemotactic response of the Tar-only strain (HCB1414-pLC113-pVS88) to four typical

concentrations of potassium. The blue line denotes the orignal signal, and the red dots represent the pH-correcting signal. **D.** The chemotactic response of the no-receptor strain (HCB1414-pVS88) to 30 mM KCl. The vertical purple (green) arrows denote the moment of adding (removing) stimulus.

Fig. 6. **A.** The oscillating spatial gradient of potassium. **B.** The dose-response curve of receptor-kinase activity to potassium. Blue dots are pH-corrected experimental data (blue dots in Fig. 4B). Red solid line is the fitting curve with Eq. 2. **C.** Typical traces of simulated mean positions with L_0=1.0 mM and T = 2 hrs. The blue and green line denote the mean x-position ($1500 - \langle x \rangle$) and mean y-position ($\langle y \rangle$), respectively. The purple dashed line indicates the oscillating potassium source at x=0. The phase delay $\Delta\phi$ is defined as the phase shift between the trough of the mean x-position and the trough of potassium source except for t/T=0. **D.** The comparison of the mean x-position under different periods of the driving source: T = 1, 2, 3 and 4 hrs. The purple dashed line indicates the oscillating potassium source at x=0. **E.** The relation between the phase delay $\Delta\phi$ and the driving period T. Each data was calculated by the average of 10 simulations. The error denotes standard deviation. **F.** The relation between lag time ($\Delta\phi \cdot T$) and the driving period T. The error denotes standard deviation.

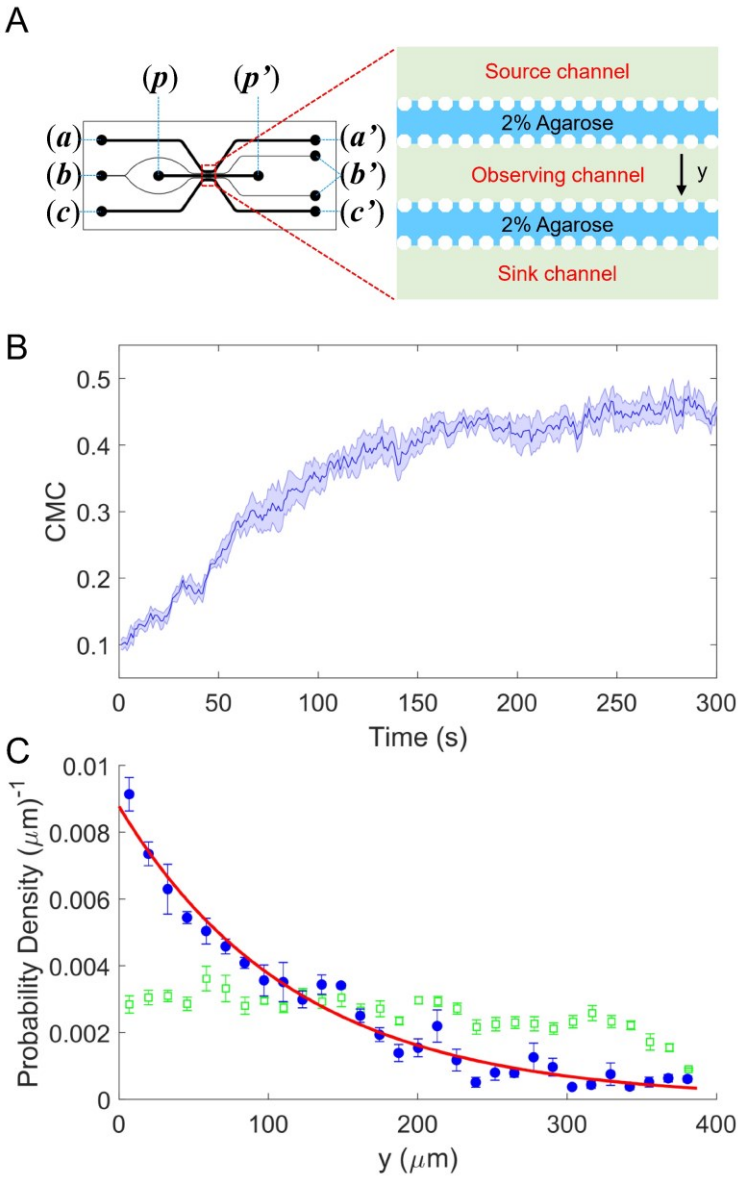

Fig. 1. The chemotaxis performance of *E. coli* in a linear concentration gradient of potassium. **A.** Design diagram of the microfluidic device. The source channel and sink were flowed with 100 mM KCl and motility buffer, respectively. The inlets of KCl, agarose, motility buffer and cells are denoted by (***a***), (***b***), (***c***) and (***p***), respectively. The outlets are labeled by the corresponding letters with the prime symbol. **B.** The average CMC of four datasets as a function of time for the wild-type strain (HCB1) under a linear concentration gradient of KCl. The shaded area denotes SEM. **C.** The cell density profile in the observing channel along the *y*-axis at the beginning ($t = 1$ s, green squares) and a steady state ($t = 300$ s, blue dots). The red solid line is an exponential fit to the data. Error bars denote SEM.

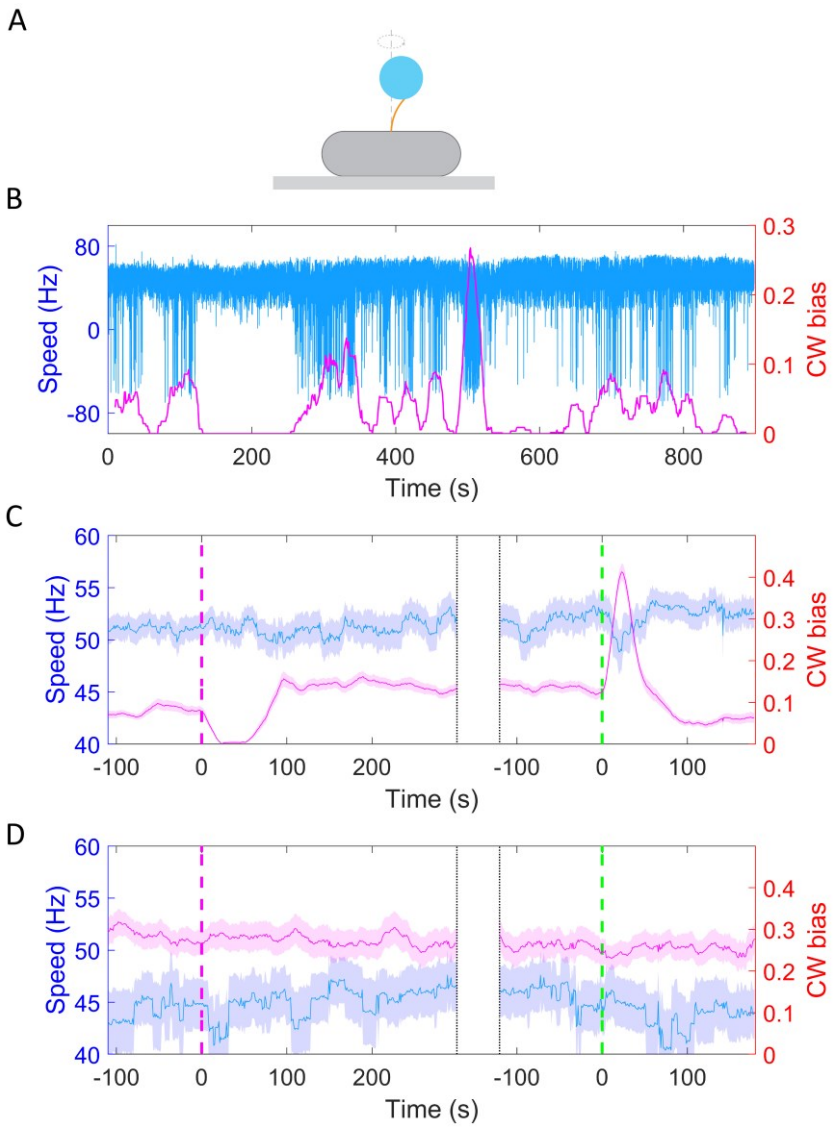

Fig. 2. The response of motor rotational signal to potassium. **A.** Schematic diagram of the bead assay for the flagellar motor. **B.** Typical trace of rotational speed (blue line) and CW bias (purple line) of individual motors for the wild-type strain (JY26-pKAF131). The positive and negative values of speed denote CCW and CW rotation, respectively. 30 mM KCl was added at t =120 s and removed at t = 480 s. **C.** The average response of 83 motors from 5 samples for the wild-type strain to 30 mM KCl. The vertical purple (green) dashed lines indicate the moment of adding (removing) stimulus. The shaded areas denote SEM. **D.** The average response of 22 motors from 4 samples for the chemotaxis-defective strain (HCB901-pBES38) to 30 mM KCl. The vertical purple (green) dashed lines indicate the moment of adding (removing) stimulus. The shaded areas denote SEM.

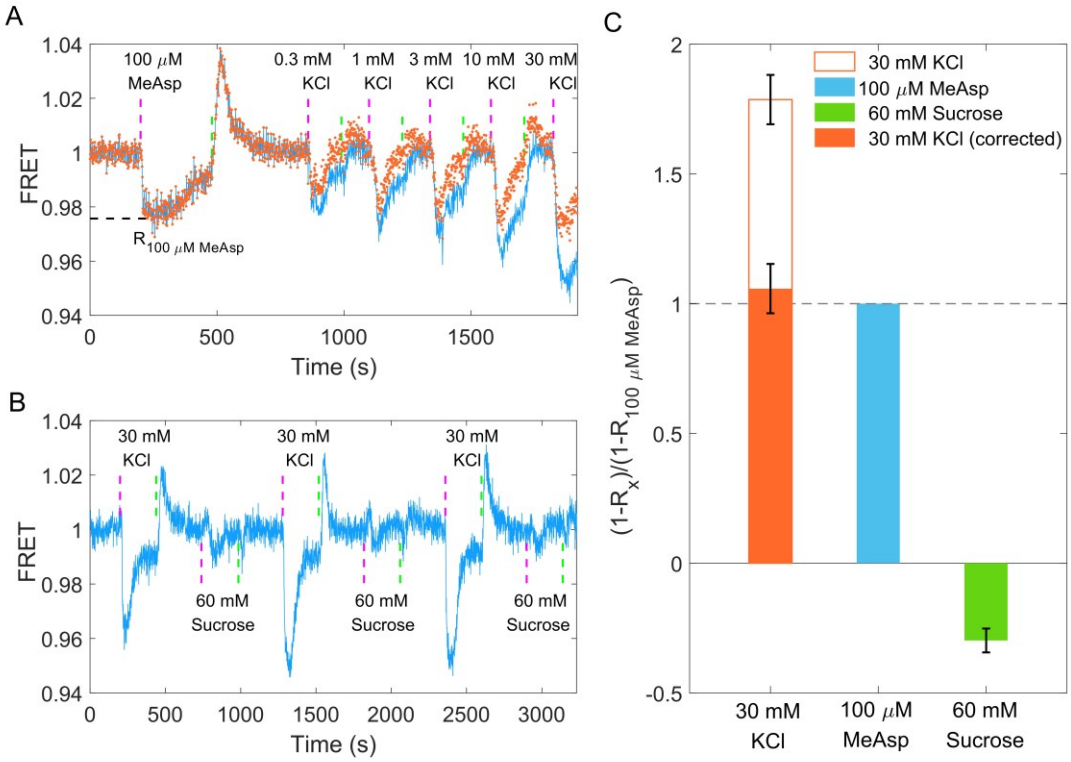

Fig. 3. The chemotactic response of the wild-type strain (HCB1288-pVS88) to potassium. **A.** Chemotactic response of the wild-type strain (HCB1288-pVS88) to stepwise addition and removal of KCl. The blue solid line denotes the orignal signal, and the red dots represent the pH-corrected signal, which was recalculated from the pH-corrected CFP and YFP channels using the response of the no-receptor strain. **B.** Comparison of the chemotactic response to 30 mM KCl and 60 mM sucrose. The vertical purple (green) dashed lines indicate the moment of adding (removing) stimulus. **C.** Quantitative comparison among the responses to 100 μM MeAsp, 30 mM KCl and 60 mM sucrose. The hollow and solid red bars represent the value calculated from the original signal and the pH-corrected signal, respectively. The errors denote SEM.

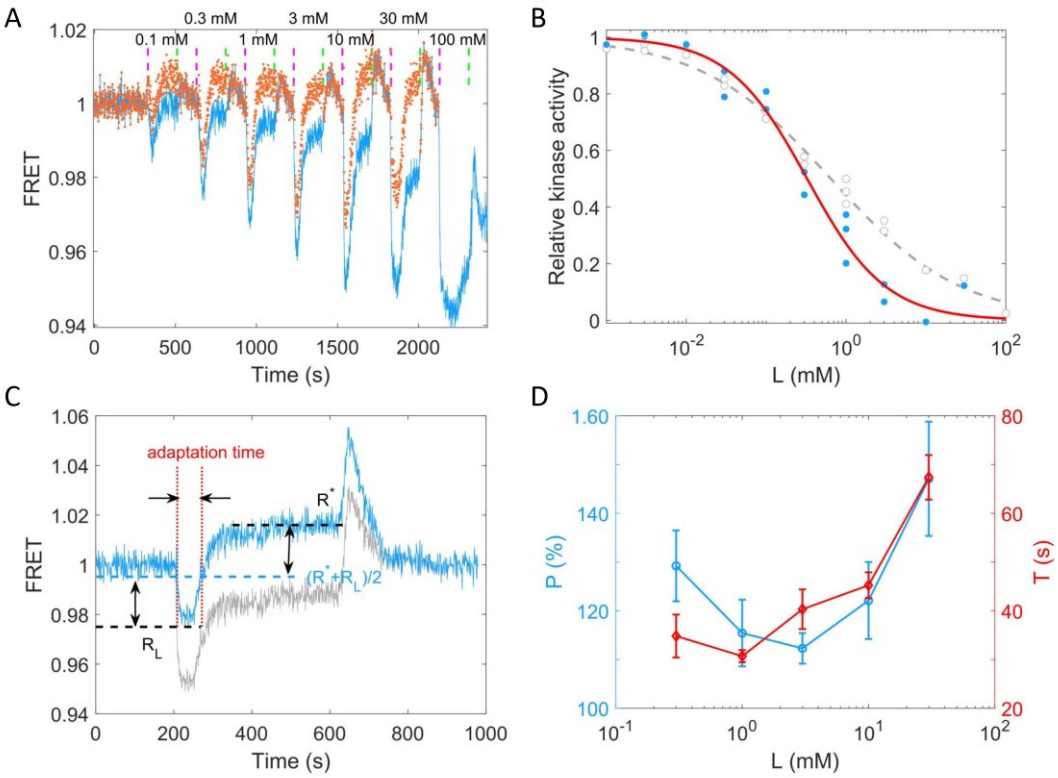

Fig. 4. Quantitative results of the chemotactic response of the wild-type strain (HCB1288-pVS88) to potassium. **A.** A typical example of the dose-response measurement. The blue solid line denotes the original signal, and the red dots represent the pH-corrected signal, recalculated from the pH-corrected CFP and YFP signals using the response of the no-receptor strain. The vertical purple (green) dashed lines indicate the moment of adding (removing) stimulus. **B.** The dose-response curve of relative kinase activity to KCl. The blue dots and gray circles represent the pH-corrected and original experimental data, respectively. The red solid and gray dashed lines are the fit curves for the blue dots and gray circles, respectively, using a Hill function. The fitted Hill coefficient for original and pH-corrected response were 0.53±0.04 and 0.88±0.14, respectively, and the concentration for half-maximal response ($K_{0.5}$) were 0.64±0.12 mM and 0.33±0.06 mM, accordingly. **C.** Definition of adaptation time in the step response. The gray and blue lines represent the original and pH-corrected signals, respectively. **D.** The adaptation level $P = (\mathrm{R}^* - \mathrm{R_L})/(1 - \mathrm{R_L})$ and adaptation time (T) as a function of the concentration of KCl, calculated with pH-corrected data. The errors denote SEM.

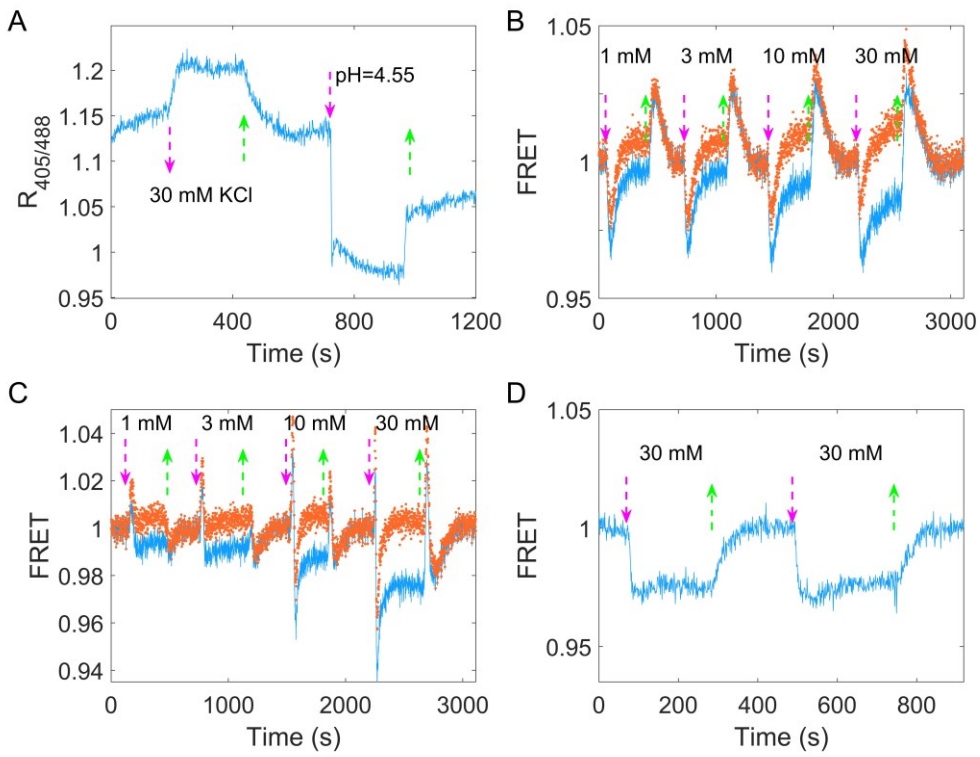

Fig. 5. **A.** The response of intracellular pH to 30 mM KCl for the wild-type strain (HCB33-pTrc99a_pHluorin2). The response to 20 mM sodium benzoate solution with pH=4.55 was used as a control. **B.** The chemotactic response of the Tsr-only strain (HCB1414-pPA114-pVS88) to four typical concentrations of potassium. The blue line denotes the orignal signal, and the red dots represent the pH-correcting signal. **C.** The chemotactic response of the Tar-only strain (HCB1414-pLC113-pVS88) to four typical concentrations of potassium. The blue line denotes the orignal signal, and the red dots represent the pH-correcting signal. **D.** The chemotactic response of the no-receptor strain (HCB1414-pVS88) to 30 mM KCl. The vertical purple (green) arrows denote the moment of adding (removing) stimulus.

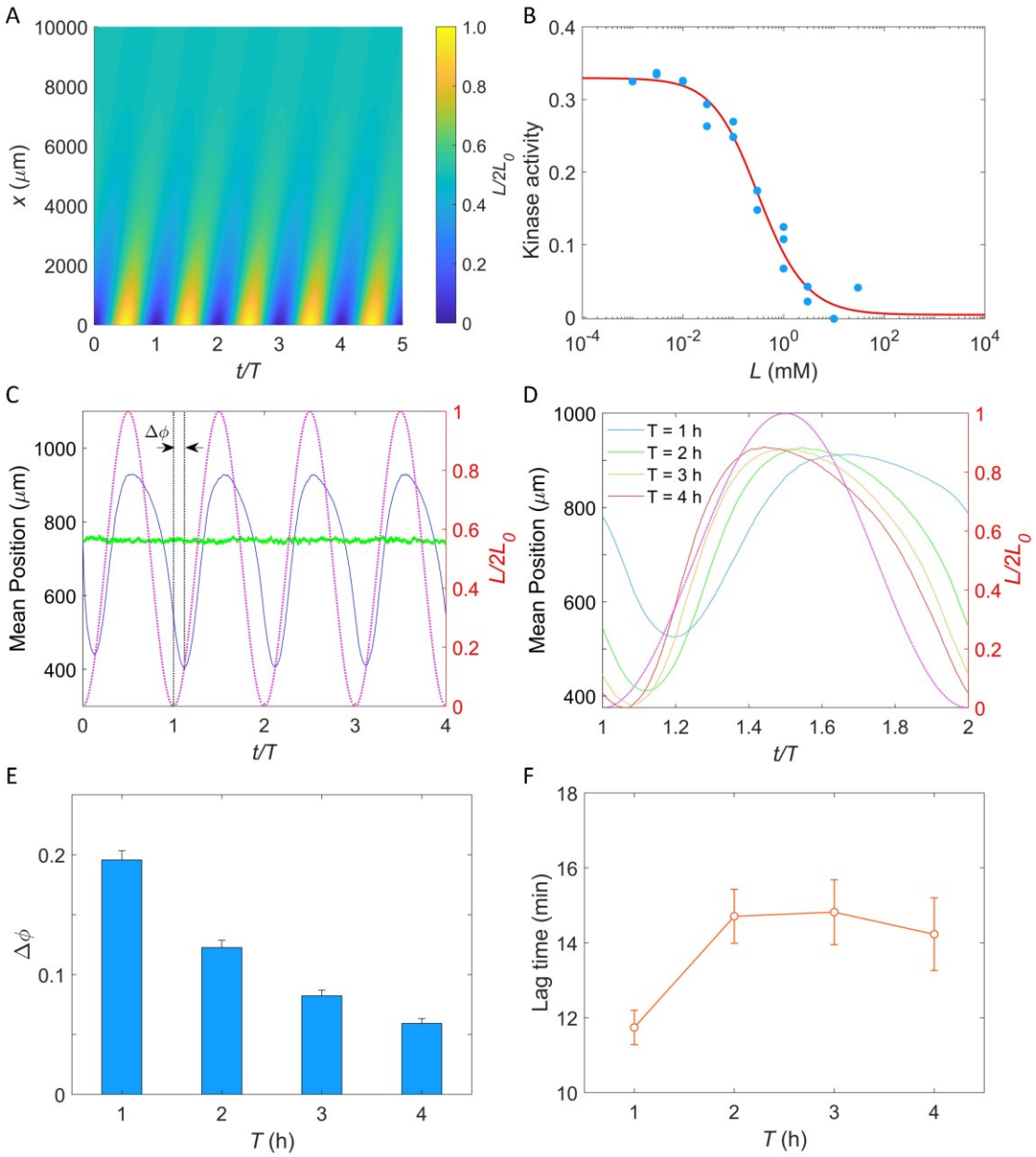

Fig. 6. **A.** The oscillating spatial gradient of potassium. **B.** The dose-response curve of receptor-kinase activity to potassium. Blue dots are pH-corrected experimental data (blue dots in Fig. 4B). Red solid line is the fitting curve with Eq. 2. **C.** Typical traces of simulated mean positions with L_0=1.0 mM and T = 2 hrs. The blue and green line denote the mean x-position ($1500 - \langle x \rangle$) and mean y-position ($\langle y \rangle$), respectively. The purple dashed line indicates the oscillating potassium source at x=0. The phase delay $\Delta\phi$ is defined as the phase shift between the trough of the mean x-position and the trough of potassium source except for t/T=0. **D.** The comparison of the mean x-position under different periods of the driving source: T = 1, 2, 3 and 4 hrs. The purple dashed

line indicates the oscillating potassium source at x=0. **E.** The relation between the phase delay $\Delta\phi$ and the driving period T. Each data was calculated by the average of 10 simulations. The error denotes standard deviation. **F.** The relation between lag time ($\Delta\phi \cdot T$) and the driving period T. The error denotes standard deviation.